Scientific Research Publishing

Open Journal of Composite Materials, 2024, 14, 147-157
https://www.scirp.org/journal/ojcm
ISSN Online: 2164-5655
ISSN Print: 2164-5612

Stiffness of *In-Situ* Formed Interleaving Polymeric Nanofiber-Epoxy Nanocomposites

Farzin Javanshour[1], Kaan Bilge[2,3], Abdul Bari Abdul Raheman[4], Melih Papila[4*]

[1]VTT Technical Research Centre of Finland Ltd., Tampere, Finland
[2]Insight Technology Development and Consultancy, Kozyatağı, Istanbul, Türkiye
[3]Materials Science & Nano Engineering Program, Sabanci University, Istanbul, Türkiye
[4]Department of Mechanical Engineering, California State University Northridge, Northridge, USA
Email: *melih.papila@csun.edu

How to cite this paper: Javanshour, F., Bilge, K., Abdul Raheman, A.B. and Papila, M. (2024) Stiffness of *In-Situ* Formed Interleaving Polymeric Nanofiber-Epoxy Nanocomposites. *Open Journal of Composite Materials*, **14**, 147-157.
https://doi.org/10.4236/ojcm.2024.144011

Received: September 19, 2024
Accepted: October 28, 2024
Published: October 31, 2024

Abstract

This study proposes a facile, but precise method to back-calculate the effective modulus of nanocomposite interleaving plies. Adaptation of a conventional dry-reinforcement resin film infusion (RFI) approach allows interleaving neat epoxy layers (NE) with the epoxy-infused nanofibrous plies (XE) of constant thickness. The final cured nanocomposite laminate thus has the form $(NE/XE)_n$, where "n" denotes the number of the repeats and enables clear distinction of the nanocomposite interlayers through the thickness. Mechanical testing of neat epoxy and laminated nanocomposite specimens can be coupled with the classical lamination theory for back-calculating in-plane elastic modulus of the individual epoxy-infused nanofibrous plies (E_{XE}). Finite element analysis (FEA) and testing the laminated nanocomposite subject to flexural loading (3-point bending) are proposed to validate the analytically back-calculated E_{XE}. It is shown that the FEA prediction incorporating E_{XE} and testing for flexural modulus of $(NE/XE)_{20}$ laminated nanocomposites correlate well and the results are within 5%. This finding suggests that the back-calculation scheme reported herein would be attractive for accurately determining the properties of an individual nanocomposite building block layer. The proposed framework is beneficial for modelling laminated structural composites incorporating XE-like nanocomposite interlayers.

Keywords

Lamination Theory, Resin Film Infusion, Electrospun Nanofibers, Mechanical Properties

1. Introduction

Interlaminar modification of fiber reinforced laminates by nonwoven polymeric

veils has been of interest for enhancing the mechanical behavior of composites. The main strategy is to interleave a self-supporting thin thermoplastic nonwoven veil between the fiber reinforced epoxy matrix prepreg plies [1] [2]. Recent studies with hybrid meltable/non-meltable thermoplastic nonwoven veils showed significant improvement on the Mode I-II fracture toughness of composites [3] [4]. For instance, Quan *et al.* [4] reported that PA-based veils enhanced the Mode-I fatigue resistance energy of unidirectional carbon-epoxy composites by 143% due to modified crack deflection and bridging mechanisms. Their polymeric interlayers were of 15 g/m^2. Once infused with an epoxy resin of the laminated composite, the individual cured thickness of veil reinforced interlayers was between 23 - 50 μm.

Lighter and thinner interleaving veils by electrospun polymeric nanofibers have also been studied. Such veils can toughen the resin-dominated interlaminar bonding lines formed between adjacent reinforcing plies of structural composites and increase their resistance to delamination [5]-[9]. These veils are porous and typically with fiber diameter in the range of 100 - 500 nm [10]. They can also be multiscale highly hybridized veils, also enabling spatially well-distributed large particles such as milled carbon fibers [11]. During the cure cycle of the hosting composite material, epoxy resin infuses into the veils, and thin nanofiber reinforced epoxy nanocomposite interlayers are formed [12]. The nanofibers preserve their nonwoven and high surface area morphology within these nanocomposite interlayers and elevate the energy required to initiate and propagate microcracks and delamination between the adjacent structural composite plies [5] [12].

Despite the growing interest in polymeric nanofiber interleaved laminated composites [13], studies reporting the mechanical properties of *in-situ*-formed individual nanocomposite interlayers themselves are lacking. This study aimed to demonstrate a straightforward yet effective hybrid (computational and experimental) characterization approach to determine their in-plane modulus. The approach combined quasi-static tensile testing of nanofiber veils embedded in the epoxy resin film adhesives and classical lamination theory (CLT). The proposed custom laminate was effectively a stack of neat epoxy and thin nanocomposite layers, meaning epoxy-infused nanofibrous veils, with constant thickness separated by neat epoxy layers. Based on the collected experimental data, CLT was then used to back-calculate the in-plane modulus of *in-situ* formed nanocomposite interlayers precisely. The flexural modulus of the (epoxy/nanocomposite)$_n$ laminated composites was finally analyzed via Solidworks 2022 Simulation module with back-calculated in-plane modulus as the material property input to compare with the flexural testing.

2. Methodology

Polymeric, PA66 electrospun nanofibrous veils (herein labelled as X) with an areal weight of 3 g/m^2 were purchased from NANOLAYR Ltd. (Auckland, New Zealand). The average diameter of PA66 electrospun nanofibers was 252 ± 40 nm.

Unsupported epoxy resin films with an aerial weight of 113 g/m^2 were purchased from c-m-p GmbH (MITSUBISHI Chemicals, Heinsberg, Germany).

The steps for producing the laminated nanocomposites are schematically described in **Figure 1**. A self-supporting ply of PA66 nanofibrous veil (X) was laid over a layer of neat epoxy resin film (NE), **Figure 1(a)** and **Figure 1(b)**. The stacking of NE and dry X-nanofiber layers was repeated until the desired configuration was achieved (see **Figure 1(c)**). A custom-made Teflon template/spacer in accordance with specific test specimen geometry (e.g., a dog-bone-shaped specimen for tension tests) was also placed on the very last layer of the stack. The final stack of nanocomposite and the template was then sandwiched between two aluminum molding plates covered with a release film. The gap between the aluminum plate edges was covered with sealant tape to avoid excessive bleed-out of the epoxy during the cure cycle. The lay-up was then vacuum bagged as shown in **Figure 1(d)** and cured using a hot press (heat-up rate of 2˚C/min till 140˚C, at 2 bars). Note that the use of template under the pressing force eliminated the need for a razor cut after the curing and associated edge cracks that might occur while cutting the test specimens. The laminated nanocomposites were denoted as $(NE/XE)_n$ where NE and XE stand for the cured neat epoxy layer and an *in-situ* cured nanocomposite layer, respectively.

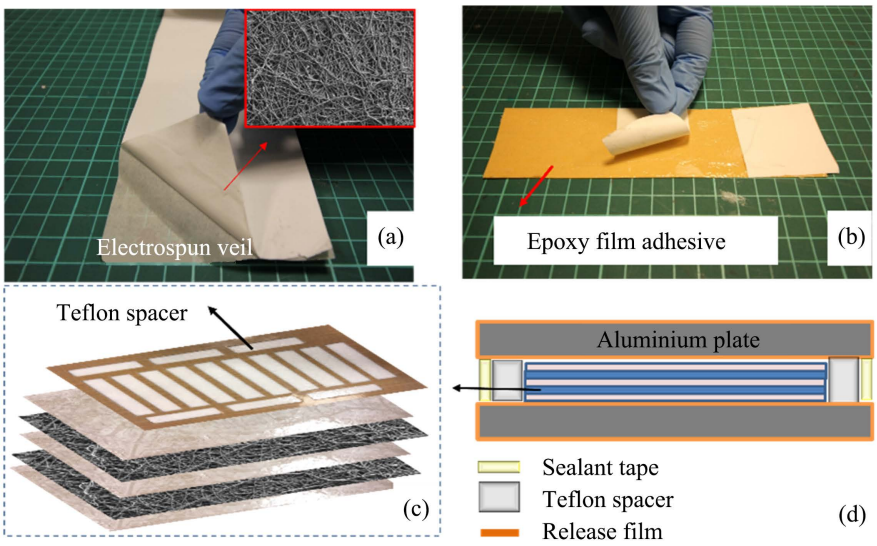

Figure 1. A schematic description for the manufacturing steps for $(NE/XE)_n$ type composites by resin film infusion. (a) Separation of veil from backing paper, (b) Hand laying of veil on neat epoxy resin film, (c) Example $(NE/XE)_2$ lay-up with Teflon template/spacer, and (d) Final stack of composite in the mold.

The tensile test specimen configuration was selected as $(NE/XE)_2$ for the laminated nanocomposite and $(NE)_3$ for the reference neat epoxy. The specimens were 0.53 ± 0.08 mm thick. The length and width of the specimens were set as 160 mm and 10 mm, respectively, in accordance with the ASTM D3039 minimum tensile specimen geometry requirements. As for the 3-point bending test, $(NE/XE)_{20}$

laminated composite and reference NE specimens with a nominal size of 100 mm × 14.5 mm × 1.4 mm (length × width × thickness) were manufactured. The PA66 nanofiber weight fraction of the processed $(NE/XE)_2$ and $(NE/XE)_{20}$ specimens was 1.1 ± 0.1 wt% and 3.7 ± 0.1 wt%, respectively.

Quasi-static tensile tests were performed using a universal testing machine (model Z100 Proline, Zwick/Roell, Ulm, Germany) in accordance with ASTM D3039. The specimens were tested by a 100 kN load cell at a 2 mm/min displacement rate. The strain was measured using a 50 mm gage clip-on extensometer. Abrasive papers were placed without glue between the gripping clamps and the specimens to avoid slipping.

The quasi-static flexural tests in 3-point bending mode were performed on the Zwick/Roell Z100 device with a 100 kN load cell following ASTM D7264. The displacement rate was 2 mm/min. The support span-to-thickness ratio was set as 20:1. For each testing series, five specimens of the $(NE/XE)_n$ nanocomposites and reference NE were tested. The flexural stress (σ_{flx}), strain (ε_{flx}) and modulus (E_{flx}) were calculated using the following equations.

$$\sigma_{flx} = \frac{3PL}{2bt^2} \tag{1}$$

$$\varepsilon_{flx} = \frac{6w_{\max}t}{L^2} \tag{2}$$

$$E_{flx} = \frac{L^3}{4bt^3}\frac{\mathrm{d}P}{\mathrm{d}w} = \frac{L^3}{4bt^3}m \tag{3}$$

where P, w, L, b, t, and m are applied flexural load, lateral displacement, length, width and thickness of the specimen, and slope of load-lateral displacement curve, respectively.

The fracture surface of the specimens was examined by using a scanning electron microscope (SEM) (model LEO 1530VP FE-SEM, Zeiss, Oberkochen, Germany). It was operated employing a secondary electron detector and in-lens detector at 2 - 5 kV after carbon coating of the specimens. Cross-sectional inspection of the $(NE/XE)_n$ nanocomposites was done with an optical microscope (model Eclipse ME 600, Nikon Co., Kogaku, Japan) to assess the distribution and thickness of individual XE layers.

3. Results and Discussions

3.1. Tensile Behavior

The contribution of XE nanocomposite layers on the tensile stress-strain curves of epoxy specimens is presented in **Figure 2(a)**. The multilayer configuration of $(NE/XE)_2$ specimens is schematically shown in **Figure 2(b)**.

The mechanical behavior of $(NE)_3$ and $(NE/XE)_2$ laminated composite specimens is summarized in **Table 1**. The in-plane tensile elastic modulus (E) of $(NE)_3$ is moderately improved by 9% on average, with the addition of PA66 nanofiber veils. Such an increase contrasts with a decrease in elastic modulus reported by

Ahmadloo *et al.* [14] for in-house electrospun PA66 nanofiber yarn-epoxy. The main difference to note is the fact that nanofibers in this study were embedded into epoxy as a planar network of nanofibers, and they reside as spatially complete layers as opposed to somewhat localized placement as a yarn by Ahmadloo *et al.* [14]. Moreover, the average values of tensile failure strength ($\sigma_{failure}$), failure strain ($\varepsilon_{failure}$), and tensile toughness for $(NE/XE)_2$ specimens are respectively 25%, 26%, and 54% higher compared to the unreinforced $(NE)_3$ epoxy specimens. It should be highlighted that the PA66 nanofibrous veils (*i.e.*, X-veils) comprised only 1.1 wt% of the $(NE/XE)_2$ specimens. The results show that incorporating distinctive XE nanocomposite layers can significantly alter the toughness of typically brittle epoxy specimens without compromising their stiffness. The toughening mechanisms in NE/XE composites are further elaborated in the next section through fractographic discussion (Section 3.2).

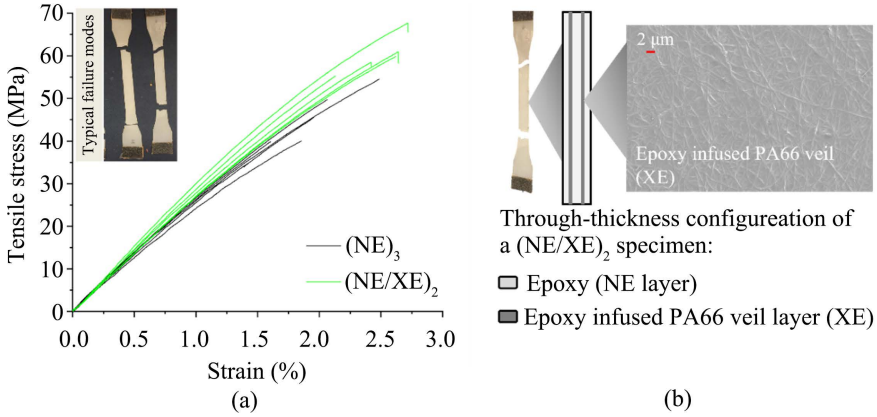

Figure 2. (a) The typical tensile stress-strain curves of neat epoxy $(NE)_3$ and $(NE/XE)_2$ laminated composites, (b) A schematic configuration of a $(NE/XE)_2$ specimen.

Table 1. The quasi-static tensile properties of specimens.

Lay-up	E (MPa)	$\sigma_{failure}$ (MPa)	$\varepsilon_{failure}$ (%)	Toughness (J/m^3)
$(NE)_3$	2758 ± 58	48 ± 5	1.9 ± 0.3	53 ± 10
$(NE/XE)_2$	3000 ± 50	60 ± 4	2.4 ± 0.3	82 ± 14

3.2. Fracture Surface Analysis of Laminated Nanocomposites

Fracture surface images of the $(NE)_3$ and $(NE/XE)_2$ nanocomposite tested in tension mode are provided in **Figure 3**. Images from the broken $(NE)_3$ (**Figure 3(a)**) specimens suggest that the fracture was due to multiple crack initiation points (depicted as yellow) at the middle and the edge of the test specimen. The fracture surface of the $(NE)_3$ specimen contains two distinct regions separated by a large hill (marked by a dashed line) with oval riverlines at its edge. The orientation of the riverlines indicates oblique crack propagation at an angle of 69˚ towards the edge of the specimen. The oblique crack propagation suggests that the final fracture is due to resultant shear failure under applied tensile loading. In **Figure 3(b)**,

the fracture surface of the $(NE/XE)_2$ specimen has two distinct regions of nanofiber reinforced (XE) and unreinforced epoxy (NE). Similar to $(NE)_3$, large hills with riverline marks at the edge are also evident in the $(NE/XE)_2$ specimen. However, in the $(NE/XE)_2$ specimen, the direction of riverlines on the hill is perpendicular to the nanofiber reinforced region (XE); hence they originate from the XE. This suggests that the XE region is a crack origin point due to the tensile stiffness mismatch with respect to NE. The orientation of the nanofiber reinforced region (XE) is at 82˚, suggesting the tensile failure mode of the XE region, which provides evidence of strength improvements reported in Table 1. The nanofiber debonding and pull-out marks in Figure 3(c) suggest effective nanofibrous reinforcement by multiscale failure mechanisms.

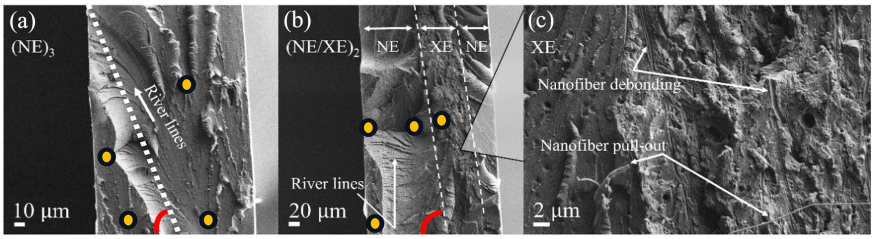

Figure 3. The tensile test specimen fracture surfaces. (a) $(NE)_3$, (b) $(NE/XE)_2$, and (c) XE.

3.3. Flexural Behavior

Through-the-thickness (*i.e.*, out of plane) view of flexural test specimens of $(NE/XE)_{20}$ configuration is presented in Figure 4. The strip patterns in Figure 4(a) and Figure 4(b) reveal the distinct individual XE nanocomposite layers with an average thickness of 22 ± 2 μm. The cross-sectional images here also confirm the success of the proposed resin film infusion (RFI) scheme in making $(NE/XE)_n$ laminated composites with well-controlled nanocomposite (*i.e.*, XE) layers. The RFI scheme in this study assures consistency in the thickness values of the distinct XE layers, which is beneficial for further analytical and numerical investigations.

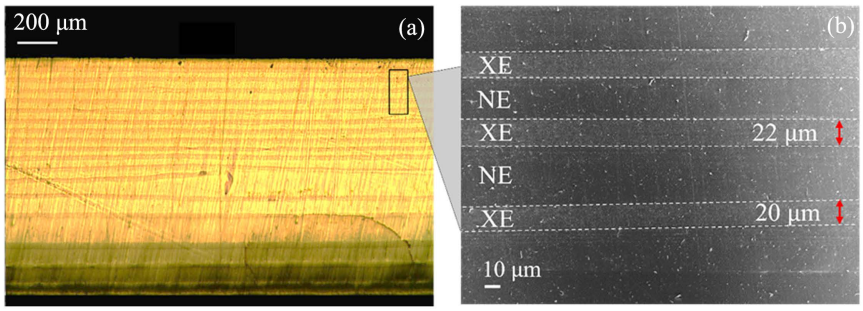

Figure 4. (a) Cross-section image from $(NE/XE)_{20}$ laminated composites conducted by a visible light microscope, (b) SEM image of neighboring XE/NE layers.

The contribution of distinctive XE nanocomposite layers on the flexural behavior of epoxy specimens is summarized in Table 2. According to the results,

integration of 20 XE layers (*i.e.*, 3.7 wt% of PA66: X nonwoven veils) alter the average flexural elastic modulus, failure strength, and elongation at failure of unmodified NE specimens by 26%, 16%, and 26%, respectively. Therefore, the average flexural toughness of $(NE/XE)_{20}$ specimens is 20% higher than $(NE)_{20}$.

Table 2. The summarized quasi-static flexural properties of specimens.

Specimen	E_{flx} (MPa)	σ_{flx} (MPa)	ε_{flx} (%)
(NE)	2900 ± 180	115 ± 5	4.1 ± 0.1
$(NE/XE)_{20}$	3660 ± 150	134 ± 10	5.2 ± 0.5

In **Figure 5**, higher ductility and toughness characteristics of $(NE/XE)_{20}$ specimens are also evident by their non-linear stress-strain behavior compared to the brittle failure mode of $(NE)_{20}$.

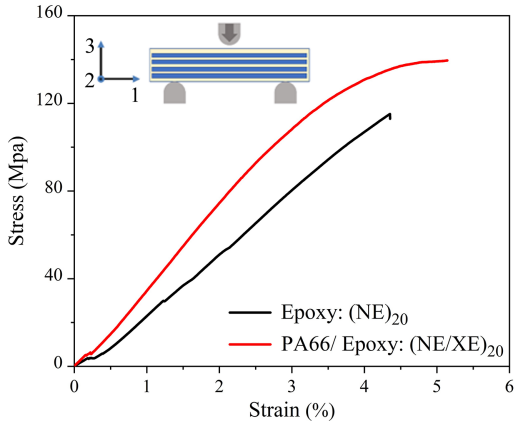

Figure 5. The typical representative flexural stress-strain curves of specimens.

In summary, the flexural and tensile test results showed that XE layers considerably enhance the mechanical behavior of epoxy. An increase in the strength was arguably anticipated the most as the XE layers of the laminated nanocomposite can suppress the cracks [12] [15] [16] as opposed to neat/bulk epoxy specimens. In-plane elastic modulus increase of the tensile test specimens (by +9%, see **Table 1**) suggested that the distinctive XE nanocomposite layers (also to call as XE building blocks, exemplified in **Figure 4**) have higher stiffness than the neat epoxy. Their dispersion through the thickness, including the layers in the vicinity of the outer surfaces, further elevated the flexural elastic modulus (+26%) compared to the neat epoxy. The flexural elastic modulus (E_{flx}) values in this section are provided as a reference value for the back-calculation of the E_{flx} within XE building blocks.

3.4. Coupling Classical Lamination Theory and Experiments for Characterization of Building-Block Nanocomposite Layer XE

The testing and framework presented in this study aim for a straightforward, but

accurate characterization approach that couples experimental results and the classical lamination theory. $(NE/XE)_n$ composite is a laminate with distinct nanocomposite layers (XE), as depicted in Figure 4. Therefore, its mechanics can be easily elaborated using the classical lamination theory (CLT) and finite element analysis (FEA) of laminated composites. In this section, the in-plane tensile elastic modulus of XE is analytically back-calculated in the scope of CLT. Then, the 3-point bending test of $(NE/XE)_{20}$ composites is simulated with FEA using Solidworks 2022 Simulation module.

The elastic modulus of the distinct cured nanocomposite building block layer (XE) is denoted as E_{XE} and can be back-calculated using the in-plane stiffness matrix of the laminated nanocomposite $(NE/XE)_n$ herein. Simplifying assumptions are the following: 1) building block, cured nanocomposite material layer XE is isotropic due to its randomly oriented nanofiber phase along with the isotropy of its epoxy matrix, 2) Poisson's ratio of XE is the same as the epoxy NE layers (0.35), 3) elastic modulus of the cured neat epoxy, E_{NE} = 2758 MPa (based on the data in Table 1), 4) elastic modulus of the cured laminated nanocomposite $(NE/XE)_n$, E_{LN} = 3000 MPa (based on the data in Table 1). Also, the average thickness of the individual XE layers (as shown in Figure 4(b) is 0.022 ± 0.002 mm. Considering $(NE/XE)_2$ composite tension test specimens and their total thickness (t_{TOT} = 0.55 mm on average), distinct epoxy layers of Figure 4 occupy a total t_{NE} = 0.506 mm thick part of the specimen. Assumptions (1) and (2) lead CLT to the following expression so that the elastic modulus of XE (E_{XE}) is:

$$E_{XE} = \frac{t_{TOT}E_{LN} - E_{NE}t_{NE}}{t_{XE}} \tag{4}$$

With the total thickness of XE plies, t_{XE} = 0.044 mm, Equation (4) results in E_{XE} = 5783 MPa. This result suggests that the in-plane tensile elastic modulus of $(NE/XE)_2$ composites in Table 1 (3000 ± 250 MPa) is not representative of the in-plane stiffness for the cured individual thin nanocomposite layers XE (epoxy resin film infused into electrospun nanofiber veils). Therefore, the back-calculation scheme presented and associated results for the building block properties would arguably be essential for further modelling and accurate predictions. To support the proposed scheme, flexural FEA analyses of the NE and $(NE/XE)_{20}$ composite specimens were performed. Static linear analysis in Solidworks 2022 Simulation Module was used to model and simulate the flexural tests in 3-point bending mode. The model used a fine standard mesh with a global size of 0.8 mm resulting total of 4964 shell elements. The experimental E_{NE} = 2758 MPa and back-calculated E_{XE} = 5783 MPa were used for building block material properties in the laminated nanocomposite. The flexural elastic modulus of $(NE/XE)_{20}$ composite E_{flx} is then calculated by Equation (3).

An example of FEA for the flexural test, along with the force-mid-point displacement curve, is given in Figure 6. Predicted and experimental results are summarized in Table 3. The flexural modulus E_{flx} predictions were performed by FEA, which considered average XE thickness homogenously distributed within the

measured total thickness of tested specimens. The average value for computationally predicted E_{flx} is within 5% of the average test data. The difference is within 1% for the neat epoxy results. These well-correlated results suggest that the coupled theory-experiment characterization of the stiffness for a nanocomposite building block layer XE is capable.

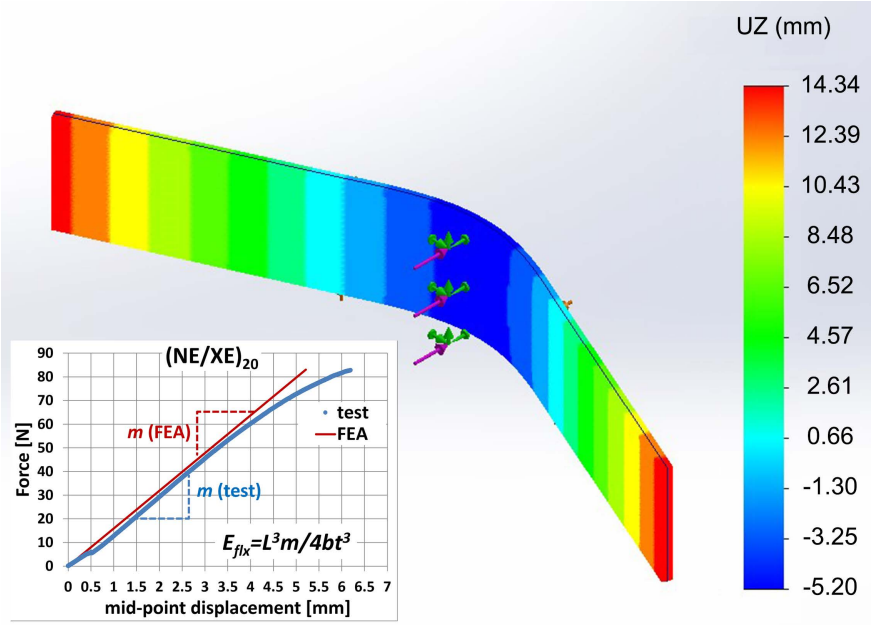

Figure 6. Finite element analysis of $(NE/XE)_{20}$ composite by 3-point bending flexural test and respective force-mid-point displacement curve.

Table 3. Flexural elastic modulus (E_{flx}) of NE and $(NE/XE)_{20}$ based on the FEA and experimental flexural tests in 3-point bending mode.

Lay-up	E_{flx} (MPa), Experimental	E_{flx} (MPa), FE analyses
(NE)	2900 ± 180	2935 ± 7
$(NE/XE)_{20}$	3660 ± 150	3836 ± 241

4. Conclusions

Laminated nanocomposites were manufactured similar to the conventional dry-reinforcement resin film infusion method by using nonwoven PA66 veils (X) and epoxy resin films (NE). Homogenized laminates had the $(NE/XE)_n$ configuration, where NE and XE represented the distinctive layers of epoxy and epoxy-infused PA66 nanocomposite (XE), respectively. The microscopy analyses revealed that the constant thickness of the XE layers was successfully achieved by the proposed RFI alike manufacturing method. The consistent XE layer thickness was essential in back-calculation of the building-block composite properties by coupling experiments and the lamination theory.

In-plane elastic modulus of the XE was back-calculated with basic classical lamination theory (CLT). The flexural moduli of NE and $(NE/XE)_{20}$ composites from

the 3-point bending experimental results were used to validate the proposed back-calculation scheme. The predictions by FEA modelling of 3-point bending test using Solidworks 2022 Simulation module correlated the experiments very well (within 5%). The laminated composite scheme herein is representative of the *in-situ* nanofibrous interlayer formation during the cure and consolidation of the prepreg-based laminated structural composites incorporating nanofiber mats. Therefore, the proposed method can help in modeling for the behavior of the nanofiber interleaved structural composites. Results also show that the PA66 nonwoven nanofibrous veils are effective and promising toughening agents. The tensile and flexural toughness of brittle epoxy specimens were enhanced by 54% and 20%, respectively, with the additional stiffness increases.

Acknowledgements

Authors thank to Materials Science and Nano-Engineering Program of Sabanci University, for the use of material characterization laboratory.

Conflicts of Interest

The authors declare no conflicts of interest regarding the publication of this paper.

References

[1] Palazzetti, R. and Zucchelli, A. (2017) Electrospun Nanofibers as Reinforcement for Composite Laminates Materials—A Review. *Composite Structures*, **182**, 711-727. https://doi.org/10.1016/j.compstruct.2017.09.021

[2] Mahato, B., Lomov, S.V., Shiverskii, A., Owais, M. and Abaimov, S.G. (2023) A Review of Electrospun Nanofiber Interleaves for Interlaminar Toughening of Composite Laminates. *Polymers*, **15**, Article 1380. https://doi.org/10.3390/polym15061380

[3] Bilge, K. and Papila, M. (2015) Interlayer Toughening Mechanisms of Composite Materials. In: Qin, Q. and Ye, J., Eds., *Toughening Mechanisms in Composite Materials*, Woodhead Publishing, 263-294. https://doi.org/10.1016/b978-1-78242-279-2.00010-x

[4] Quan, D., Alderliesten, R., Dransfeld, C., Murphy, N., Ivanković, A. and Benedictus, R. (2020) Enhancing the Fracture Toughness of Carbon Fibre/Epoxy Composites by Interleaving Hybrid Meltable/Non-Meltable Thermoplastic Veils. *Composite Structures*, **252**, Article 112699. https://doi.org/10.1016/j.compstruct.2020.112699

[5] Quan, D., Murphy, N., Ivanković, A., Zhao, G. and Alderliesten, R. (2022) Fatigue Delamination Behaviour of Carbon Fibre/Epoxy Composites Interleaved with Thermoplastic Veils. *Composite Structures*, **281**, Article 114903. https://doi.org/10.1016/j.compstruct.2021.114903

[6] Quan, D., Bologna, F., Scarselli, G., Ivankovic, A. and Murphy, N. (2020) Interlaminar Fracture Toughness of Aerospace-Grade Carbon Fibre Reinforced Plastics Interleaved with Thermoplastic Veils. *Composites Part A*: *Applied Science and Manufacturing*, **128**, Article 105642. https://doi.org/10.1016/j.compositesa.2019.105642

[7] Beylergil, B., Tanoğlu, M. and Aktaş, E. (2018) Effect of Polyamide-6,6 (PA 66) Nonwoven Veils on the Mechanical Performance of Carbon Fiber/Epoxy Composites. *Composite Structures*, **194**, 21-35. https://doi.org/10.1016/j.compstruct.2018.03.097

[8] Bilge, K., Venkataraman, S., Menceloglu, Y.Z. and Papila, M. (2014) Global and Local Nanofibrous Interlayer Toughened Composites for Higher in-Plane Strength. *Composites Part A*: *Applied Science and Manufacturing*, **58**, 73-76. https://doi.org/10.1016/j.compositesa.2013.12.001

[9] Bilge, K., Ozden-Yenigun, E., Simsek, E., Menceloglu, Y.Z. and Papila, M. (2012) Structural Composites Hybridized with Epoxy Compatible Polymer/MWCNT Nanofibrous Interlayers. *Composites Science and Technology*, **72**, 1639-1645. https://doi.org/10.1016/j.compscitech.2012.07.005

[10] Zucchelli, A., Focarete, M.L., Gualandi, C. and Ramakrishna, S. (2010) Electrospun Nanofibers for Enhancing Structural Performance of Composite Materials. *Polymers for Advanced Technologies*, **22**, 339-349. https://doi.org/10.1002/pat.1837

[11] Asghari Arpatappeh, F., Manga, E., Bilge, K., Aydemir, B.E., Gülgün, M.A. and Papila, M. (2022) Morphology Evolution of Self-Same Nanocomposites Hybridized with Jumbo-Sized Particles. *Journal of Applied Polymer Science*, **139**, e53073. https://doi.org/10.1002/app.53073

[12] Bilge, K., Yorulmaz, Y., Javanshour, F., Ürkmez, A., Yılmaz, B., Şimşek, E., *et al.* (2017) Synergistic Role of *in-situ* Crosslinkable Electrospun Nanofiber/Epoxy Nanocomposite Interlayers for Superior Laminated Composites. *Composites Science and Technology*, **151**, 310-316. https://doi.org/10.1016/j.compscitech.2017.08.029

[13] Sasidharan, S. and Anand, A. (2022) Interleaving in Composites for High-Performance Structural Applications. *Industrial & Engineering Chemistry Research*, **62**, 16-39. https://doi.org/10.1021/acs.iecr.2c03061

[14] Ahmadloo, E., Gharehaghaji, A., Latifi, M., Saghafi, H. and Mohammadi, N. (2018) Effect of PA66 Nanofiber Yarn on Tensile Fracture Toughness of Reinforced Epoxy Nanocomposite. *Proceedings of the Institution of Mechanical Engineers*, *Part C*: *Journal of Mechanical Engineering Science*, **233**, 2033-2043. https://doi.org/10.1177/0954406218781910

[15] Daelemans, L., van der Heijden, S., De Baere, I., Rahier, H., Van Paepegem, W. and De Clerck, K. (2016) Damage-Resistant Composites Using Electrospun Nanofibers: A Multiscale Analysis of the Toughening Mechanisms. *ACS Applied Materials & Interfaces*, **8**, 11806-11818. https://doi.org/10.1021/acsami.6b02247

[16] Meireman, T., Daelemans, L., Rijckaert, S., Rahier, H., Van Paepegem, W. and De Clerck, K. (2020) Delamination Resistant Composites by Interleaving Bio-Based Long-Chain Polyamide Nanofibers through Optimal Control of Fiber Diameter and Fiber Morphology. *Composites Science and Technology*, **193**, Article 108126. https://doi.org/10.1016/j.compscitech.2020.108126